Hindawi Publishing Corporation
Journal of Spectroscopy
Volume 2016, Article ID 5184542, 9 pages
http://dx.doi.org/10.1155/2016/5184542

Research Article

Studies on Structural and Morphological Properties of Multidoped Ceria $Ce_{0.8}Nd_{0.0025}Sm_{0.0025}Gd_{0.005}Dy_{0.095}Y_{0.095}O_{2-\delta}$ ($x = 0.2$) as Solid Solutions

Marija Stojmenović,[1] Maja C. Pagnacco,[2] Vladimir Dodevski,[1] Jelena Gulicovski,[1] Milan Žunić,[3] and Snežana Bošković[1]

[1]*Institute of Nuclear Sciences "Vinča", University of Belgrade, Mihaila Petrovića-Alasa 12-14, 11001 Belgrade, Serbia*
[2]*Faculty of Physical Chemistry, University of Belgrade, Studentski Trg 12–16, 11158 Belgrade, Serbia*
[3]*Physical Sciences and Engineering Division, King Abdullah University of Science and Technology (KAUST), Thuwal 23955-6900, Saudi Arabia*

Correspondence should be addressed to Maja C. Pagnacco; maja.milenkovic@ymail.com

Received 2 February 2016; Revised 11 March 2016; Accepted 17 April 2016

Academic Editor: Eugen Culea

The nanopowdery solid solutions of multidoped ceria $Ce_{0.8}Nd_{0.0025}Sm_{0.0025}Gd_{0.005}Dy_{0.095}Y_{0.095}O_{2-\delta}$ ($x = 0.2$) with the fluorite type crystal structure of CeO_2 were synthesized for the first time. Two synthesis procedures were applied: the modified glycine-nitrate procedure (MGNP method) and room temperature self-propagating reaction (SPRT method). All nanopowders were characterized by XRPD analysis, Raman spectroscopy, low temperature nitrogen physisorption, TEM, and SEM methods. According to the XRPD and Raman spectroscopy results, single phase solid solutions of fluorite structure were evidenced regardless of the number of dopants and synthesis procedure. Both XRPD and TEM were analyses evidenced nanometer particle dimensions. The SPRT method results in obtaining sample with higher specific surface area, smaller crystallite and particles sizes, and the same values of the lattice parameter in comparison to pure CeO_2. Raman spectroscopy was confirmed to the oxygen vacancies introduced into the ceria lattice when Ce^{4+} ions were replaced with cations (dopants) of lower valence state (3+), which may indicate the potential improvement of ionic conductivity. Additionally, the presence of oxygen vacancies in the lattice ceria, as well as very developed grain boundaries, gives a new possibility for potential application of obtained nanopowders in the area of room temperature ferromagnetism as spintronics.

1. Introduction

Multiple applications of materials based on cerium (IV) oxide (CeO_2) during the past years in field electronics [1, 2], environmental protection [3, 4], optics [3–5], catalysis [6–10], and clean energy [11–13] attracted the attention of many researchers, which conditioned the CeO_2 to be the focus of interest. Great attention has been devoted to the development of a new generation nanosized solid solutions for solid oxide fuel cells (SOFCs) [12, 13], as well as for spintronic devices [14–17], where pure and doped CeO_2 have also found their application. The new generation of SOFCs should be able to operate at much lower temperatures with rather high efficiency and high ionic conductivity, as compared with currently developed ones. On the other hand, for development of a new generation of spintronics based on CeO_2, necessary is that synthesized nanopowders show good ferromagnetic properties at room temperature [14, 16]. Therefore, there is a demand for new materials that will fulfill the necessary conditions for the above said application. In addition, the materials should be less expensive, produced by the application of low cost technologies, including starting powders production.

Thus, ultrafine CeO_2 nanopowder doped with rare earth ions appears to be very interesting ceramic electrolyte for SOFCs. High ionic conductivity on lower temperature is achieved as the result of the appearance of oxygen vacancies in the cerium lattice. The phenomena of vacancies exist because of their placement of (IV)—valent cerium ions (Ce^{4+}) with rare earth (III)—valent ions [18]. Besides, it is known that the conductivity of nanocrystalline materials increases with smaller grains, and distribution becomes more uniform. This represents important precondition for considerable decrease of sintering temperature and energy loss in the process of fuel cells production. In order to enable the development of compositions with high ionic conductivity, necessary for good electrolytes, many problems have to be solved starting with those related to powder synthesis. On the other hand, as mentioned, ultrafine CeO_2 nanopowder doped with rare earth ions is promising material and for future spintronics. However, the mechanisms of ferromagnetic behavior in pure and doped CeO_2 are subject of intensive research [14–17]. The obtained experimental results are quite contradictory and strongly depend on lots of factors, such as grain size, used dopants, and its concentration, as well as synthesis method of pure or doped CeO_2. Some studies appropriately reported about correlation ferromagnetic mechanism with oxygen vacancies and defects in crystallite lattice [14, 16, 17], while on the other hand there are apparent indications that the specific grain boundary area plays an important role for ferromagnetism [19, 20]. In order to enable the development of compositions with high ionic conductivity necessary for good electrolytes and with corresponding structural, morphological, and magnetical properties necessary for good spintronics, many problems have to be solved starting with those related to powder synthesis.

The most promising methods that have a number of advantages over conventional methods [21–23] are the modified glycine-nitrate procedure (MGNP method) [24–27] and room temperature self-propagating reaction (SPRT method) [24–26]. Contrary to other methods [21–23], both MGNP and SPRT methods are very fast and reliable, whereby the required equipment is extremely simple and inexpensive. In the MGNP procedure, partial replacement of nitrate with acetate ions is done in order for the chemical reaction to be controlled better, but also to lower the cost of the process. The SPRT procedure is based on self-propagating room temperature reaction between metal nitrates and sodium hydroxide, wherein the reaction is spontaneous and terminates extremely fast. It is known that the method assures very precise stoichiometry of the final product in comparison with a tailored composition [25–27].

Bearing the abovementioned in mind, the subject of our present study was the preparation and characterization of multidoped ceria $Ce_{0.8}Nd_{0.0025}Sm_{0.0025}Gd_{0.005}Dy_{0.095}Y_{0.095}O_{2-\delta}$ ($x = 0.2$) samples as new materials for potential solid electrolytes for SOFCs and potential solid solutions for spintronics. The syntheses based on two different methods and properties comparison of obtained multidoped ceria nanopowders ($Ce_{0.8}Nd_{0.0025}Sm_{0.0025}Gd_{0.005}Dy_{0.095}Y_{0.095}O_{2-\delta}$) were presented. The potential application of mentioned materials based on CeO_2 is aimed at improving the performance of SOFCs and spintronics such as high efficiency, low working temperatures, and cost of production without environmental pollution. In this paper, the overall mole fraction (x) of dopants was kept constant ($x = 0.2$). This concentration is the optimum concentration for many dopant cations in fluorite ceria lattice [25–27].

2. Experimental

2.1. Synthesis by MGNP Method. The sample of above-mentioned composition was synthesized in the form of nanopowders by the MGNP method starting from δ-amino acetic acid-glycine (NH_2CH_2COOH) (Fluka), solution containing $Ce(NO_3)_4$ and $Ce(CH_3COO)_4$ in the 1 : 1 molar ratio, and a solution of nitrates of the $[Me(NO_3)_3{\cdot}6H_2O]$ formula, where Me stands for Ce, Nd, Sm, Gd, Dy, and Y (Aldrich), applied in the amounts necessary to assure their total concentrations in the final product to be $x = 0.2$. The reaction was carried out in a completely clean steel reactor, where all reactants were dissolved in distilled water and put simultaneously into the reactor. The concentration of metal nitrate solution required to obtain targeted composition of the final doped powder was calculated from

$$\begin{aligned} &4NH_2CH_2COOH + 2\left[(1-x)\,Ce\left(NO_3\right)_3 \cdot 6H_2O\right. \\ &\quad \left. + xMe\left(NO_3\right)_3 \cdot 6H_2O\right] + 2O_2 \longrightarrow \\ &2Ce_{1-x}Me_xO_{2-\delta} + 22H_2O\uparrow + 5N_2\uparrow + 8CO_2\uparrow \end{aligned} \tag{1}$$

The prepared solution was first heated at 90°C to remove water and further to 540°C, which was followed by calcination at 600°C over a period of 4 h to remove any remaining organic components. In the MGNP process, partial replacement of nitrate with acetate salt was done in order to slow down the reaction rate and minimize the losses of the reactants by sprinkling. The quantity of the experimentally obtained powders using the MGNP method of synthesis was very close to the theoretically calculated values (96–99%) and significantly higher than the amount of powders that had been obtained by other methods [21–23].

2.2. Synthesis by SPRT Method. Nanopowder of the $Ce_{0.8}Nd_{0.0025}Sm_{0.0025}Gd_{0.005}Dy_{0.095}Y_{0.095}O_{2-\delta}$ composition was also obtained by the SPRT method. The initial reactants were nitrate salts of Ce, Nd, Sm, Gd, Dy, and Y (Aldrich) and NaOH (Vetprom chemicals). The amounts of reactants required for the synthesis were calculated according to the following equation:

$$\begin{aligned} &2\left[(1-x)\,Ce\left(NO_3\right)_3 \cdot 6H_2O + xMe\left(NO_3\right)_3 \cdot 6H_2O\right] \\ &\quad + 6NaOH + \left(\frac{1}{2} - \delta\right)O_2 \\ &\longrightarrow 2Ce_{1-x}Me_xO_{2-\delta} + 6NaNO_3 + 15H_2O \end{aligned} \tag{2}$$

The reactants were mixed in an alumina mortar for 15 minutes, enabling rapid progress of the reaction at room temperature in air. Exposure to air for additional 3 h provided the completion of the reaction according to (2). The essence

of this method is an exothermic reaction in solid state, yielding the ceramic powders at a temperature close to room temperature. Then, the obtained suspension was transferred to a test tube containing certain amount of distilled water and subjected to centrifugation at 3000 rpm, for 10 minutes. A Centurion 1020D centrifuge was used. Rinsing procedure was repeated four times with water and twice with ethanol. The synthesized nanopowders were then subjected to drying in an oven at 100°C. The resulting powders had the expected stoichiometry. This method is pronouncedly cost-effective comparing with other methods [21–23].

2.3. Sample Characterization. The $Ce_{0.8}Nd_{0.0025}Sm_{0.0025}Gd_{0.005}Dy_{0.095}Y_{0.095}O_{2-\delta}$ powders obtained by the MGNP and SPRT methods were characterized by X-ray power diffraction (XRPD), Raman spectroscopy, low temperature nitrogen physisorption, transmission electron microscopy (TEM), scanning electron microscopy (SEM), and energy dispersive X-ray spectroscopy (EDS).

For X-ray powder diffraction (XRPD) with Cu $K_{\alpha 1,2}$ radiation an Ultima IV Rigaku diffractometer was used, equipped with a voltage generator (40.0 kV) and a current generator (40.0 mA). The range of 20–80° 2θ was used for all synthesized powders in a continuous scan mode with the scanning step of 0.02° and at the scan rate of 2°/min. Before the measurements the angular correction was done by high quality Si standard. Lattice parameters were refined from the data using the least square procedure. Standard deviation was about 1%. The internal microstrain of the samples was estimated from the Williamson-Hall plots which were drawn using the following equation [28]:

$$\beta_{\text{total}} \cdot \cos\theta = 0.9\frac{\lambda}{D} + 4\frac{\Delta d}{d} \cdot \sin\theta, \tag{3}$$

where β_{total} is the full width half maximum of the XRPD peak, λ is the incident X-ray wavelength, θ is the diffraction angle, D is the crystallite size, and Δd is the difference of the d spacing corresponding to a typical peak.

Raman spectra excited with a diode pumped solid state high-brightness laser (532 nm) were collected on a DXR Raman microscope (Thermo Scientific, USA), equipped with an Olympus optical microscope and a CCD detector. The measurements were performed at room temperature in the 200–800 cm^{-1} spectral range. The powdered sample was placed on an X-Y motorized sample stage. The laser beam was focused on the sample using 10× objective magnification. The scattered light was analyzed by the spectrograph with a 900 lines/mm grating. Laser power was kept at 1 mW.

The transmission electron microscopy (TEM) analysis of the obtained powders and their particles size was measured by a JEOL JEM-2100 (voltage: 200 kV; illumination mode: TEM; operation mode: IMAGING). Particle size was measured on micrographs directly after they had been taken using the existing computer digital micrograph software. The micrographs with as much as possible isolated particles were chosen for the measurements. The diameter of the particles was measured manually, on a computer, and the result was recalculated into particle sizes using the digital micrograph software. Approximately 40 particles were measured for each sample. The mean value was taken as the particle size of the relevant powder.

The specific surface areas of the powders were determined by the Brunauer, Emmett, and Teller (BET) method, based on the adsorption and desorption isotherms of N_2 at −196°C, as the function of relative pressure. The measurements were performed using the home made gravimetric McBain equipment, with quartz spiral of the sensitivity 0.2 mm mg^{-1}. Before the measurement, the sample was degassed at 120°C and vacuumed over 24 h. The achieved vacuum was measured with a Pirani vacuum gauge (measurement range 5.6×10^{-3}–1×10^{3} mbar, 2% measurement error for the pressure of $\leq 10^{-2}$ mbar). In the mbar range, the pressure measurement was checked with a mercury manometer. Beside the specific surface area, the pore size distribution, specific surface area of mesopore, and micropore volume were also calculated from the isotherms. Pore size distribution was obtained by applying Barrett-Joyner-Halenda (BJH) method [29] to the desorption branch of the isotherms. The specific surface area of mesopore and micropore volume was estimated using the high resolution α_s-plot method [30–32]. The specific surface area of micropore was calculated by subtracting specific surface area of mesopore from specific surface area obtained by BET method.

For scanning electron microscopy (SEM) analysis, the electron microscope model FE-SEM JEOL JSM 6330F (Japan) was used. Before the observation, the samples were precoated with a several nanometers thick layer of gold, using a Fine Coat JFC-1100 ION SPUTTER Company JEOL. The images were recorded in SEI mode at the ×10 k magnification with the accelerating voltage of 10 kV. The energy dispersive X-ray spectroscopy (EDS) analysis was carried out at the invasive electron energy of 30 keV by means of a QX 2000S device, product of the Oxford Microanalysis Group. The maximum resolution was 0.4 nm.

3. Results and Discussion

3.1. Structure Details of Nanopowders. Figure 1(a) displays the X-ray diffraction patterns for both multidoped $Ce_{0.8}Nd_{0.0025}Sm_{0.0025}Gd_{0.005}Dy_{0.095}Y_{0.095}O_{2-\delta}$ nanopowders obtained by the MGNP and SPRT methods. According to the XRPD analysis, all the peaks of the nanopowders exhibited the presence of single phase ceria with the cubic fluorite structure (space group *Fm3m*) without any other traces, demonstrating that the CeO_2 was fully stabilized by Nd_2O_3, Sm_2O_3, Gd_2O_3, Dy_2O_3, and Y_2O_3. This means that dopant ions very easily replaced the Ce^{4+} ions in the crystal lattice, because all dopants in 3+ oxidation state have the similar ionic radii as Ce^{4+} ion (0.97 Å) [33]. Thus, the additional peaks from dopants amorphous phase have not appeared (Figure 1(a)). However, one reason for absence of peaks of the amorphous phase may be the fact that XRPD (or TEM, Section 3.2) can register the diffraction only from the bulk phases. It is possible that the second components, dopant ions, segregated in the thin surface or interface layers remain invisible for XRPD. Namely, the XRPD peaks of a second phase can appear only in the case where the

Table 1: Lattice parameter (a_{XRPD}), crystallite size (D_{XRPD}), and microstrain (e_{XRPD}) obtained by the XRPD analysis and particle size obtained by the TEM analysis, for the $Ce_{0.8}Nd_{0.0025}Sm_{0.0025}Gd_{0.005}Dy_{0.095}Y_{0.095}O_{2-\delta}$ nanopowders synthesized by the MGNP and SPRT methods.

Composition	a_{XRPD} (Å)	D_{XRPD} (nm)	e_{XRPD} (%)	Particle size (nm)
MGNP method				
$Ce_{0.8}Nd_{0.0025}Sm_{0.0025}Gd_{0.005}Dy_{0.095}Y_{0.095}O_{2-\delta}$	5.4133	10.31	2.45	9.56
SPRT method				
$Ce_{0.8}Nd_{0.0025}Sm_{0.0025}Gd_{0.005}Dy_{0.095}Y_{0.095}O_{2-\delta}$	5.4142	3.52	0.49	3.17

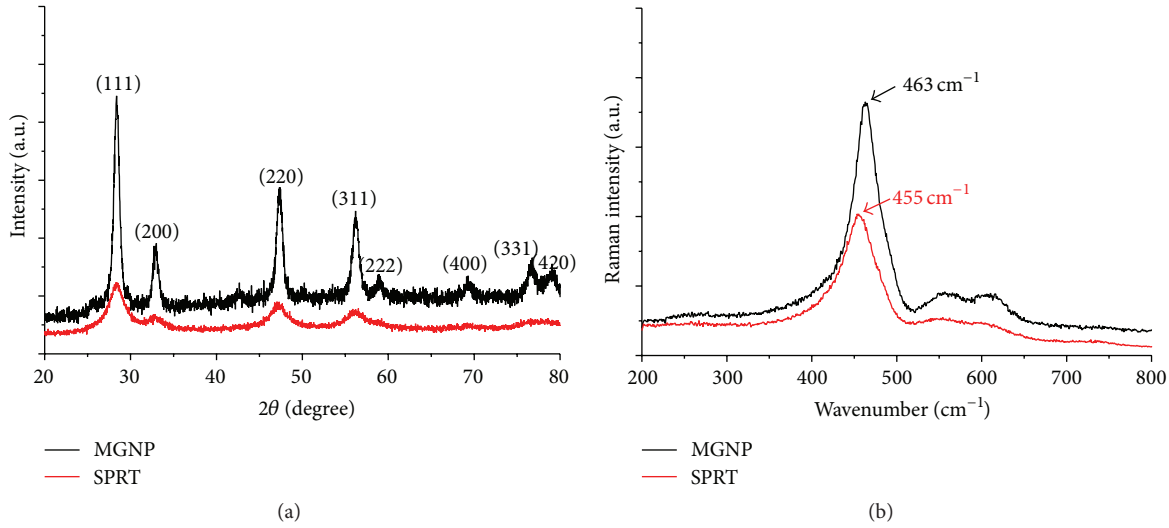

Figure 1: (a) X-ray diffraction patterns and (b) Raman spectra of the $Ce_{0.8}Nd_{0.0025}Sm_{0.0025}Gd_{0.005}Dy_{0.095}Y_{0.095}O_{2-\delta}$ nanopowders obtained by the MGNP and SPRT methods.

coherent scattering region for X-rays is large enough or when the amount of a second phase is high enough [20]. Besides, although the diffraction lines of the sample obtained by the MGNP method (Figure 1(a)) were much sharper and stronger, the powder was of the nanometer size (about 10 nm). Broader diffraction peaks for the sample synthesized using the SPRT method (Figure 1(a)) indicate smaller crystallite size and/or the presence of strain (Table 1). Due to pronounced broadening of diffraction lines of the SPRT sample, some crystal planes remained unnoticeable (*hkl*: 222, 400, 331, 420).

Bearing in mind that lattice parameter can be a useful tool for the indication of behavior of the obtained nanopowders, this parameter for both of the multidoped nanopowders based on CeO_2 obtained by the MGNP and SPRT methods was experimentally measured using the XRPD analysis (Table 1). Generally, it can be noticed that the values of lattice parameters of the multidoped samples synthesized by the MGNP method are similar to the corresponding lattice parameters of pure CeO_2 (5.4129 Å) [24]. The similar tendency, in comparison with pure CeO_2 obtained by the SPRT method (5.4143 Å) [24], is also observed for the high multidoped samples synthesized by the SPRT method. It is obvious that the experimentally obtained lattice parameter values of the doped CeO_2 in comparison with those of pure CeO_2 obtained by the MGNP and SPRT methods are in quite good agreement (Table 1), which was the aim. Namely, the primary purpose of doping was the introduction of oxygen vacancies in the crystal lattice of CeO_2 (replacement of Ce^{4+} with trivalent dopants) in order to reach higher ion conductivity, while retaining the values of the lattice parameter similar to that of pure CeO_2 [24], which was obviously achieved.

It can be noticed that, according to the XRPD analysis, the crystallite size of the sample obtained by the SPRT method is about three times smaller in comparison with the sample synthesized using the MGNP method (Table 1). Besides, it is interesting to note that the nanopowder with particle size of about 3 nm obtained by the SPRT method has the lattice parameter similar to that of the MGNP powder with particles of about 10 nm in size (Table 1). These findings suggest the possibility that powders synthesized by SPRT method have large specific grain boundary, whose area plays an important role in ferromagnetic behavior. The obtained results are in agreement with the literature data concerning the anomaly of relatively strong increase of ceria lattice parameter noticed when the particle size decreased below 10 nm [34–36]. This anomaly is ascribed to increased concentration of Ce^{3+} ions with larger ionic radius [34–36]. Besides, the nanopowder obtained by the SPRT method retained several orders of magnitude smaller value of microstrain, comparing with the powder obtained by the MGNP method. All the abovementioned indicates increased level of defects in the structure of the nanopowders, which further may increase the electric conductivity, as well as improved ferromagnetic behavior of the doped CeO_2.

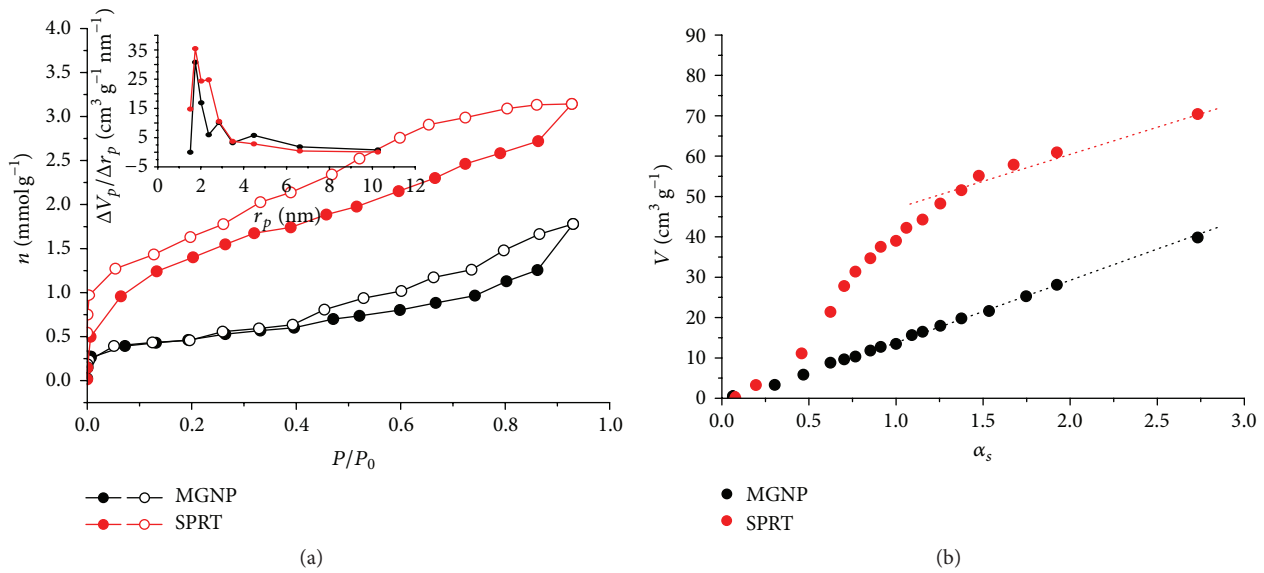

FIGURE 2: (a) Nitrogen physisorption isotherms, as the amount of N_2 adsorbed/desorbed as the function of relative pressure (solid symbols, adsorption, open symbols, desorption; inset: pore size distribution (PSD)), and (b) α_s-plots for nitrogen adsorption isotherm, of the $Ce_{0.8}Nd_{0.0025}Sm_{0.0025}Gd_{0.005}Dy_{0.095}Y_{0.095}O_{2-\delta}$ nanopowders obtained by the MGNP and SPRT methods.

The identification of the Raman spectrum, especially Raman signature for O^{2-} vacancies, is very important for characterizing solid electrolytes based on CeO_2. It is known that pure and stoichiometric CeO_2 with fluorite structure has only a single allowed Raman mode of the first order (with F_{2g} symmetry) positioned at the frequency of 465 cm^{-1} [24]. This mode was assigned as the symmetric breathing mode of O atoms around each cation (CeO_8, the lattice vibration). In the presented doped nanocrystalline CeO_2 samples experience an asymmetrical broadening in comparison with its bulk counterpart. Phonon confinement, inhomogeneous strain, and the presence of defects cause the observed changes of the Raman spectra [16]. Besides, at about 550 and 600 cm^{-1} two additional Raman modes of the second order occur [25, 26]. Namely, with particle size decreasing, the overall free surface of the powder increases enabling easier release of oxygen from the lattice, leaving the vacancy and two electrons localized on cerium atoms. This process causes the formation of Ce^{3+} ions (lowering of Ce^{4+} valence, which is due to electroneutrality demands) and the emergence of the Raman mode at around 600 cm^{-1}. On the other hand, for the doped nanopowders additional Raman mode at around 550 cm^{-1} was attributed to oxygen vacancies introduced into the ceria lattice when Ce^{4+} ions are replaced with cations of lower valence state (all dopants have oxidation numbers 3+). According to the literature [37], the intensity of these peaks at 550 and 600 cm^{-1} depends on the number of vacancies and their appearance (Figure 1(b)) may indicate potential improvement of ionic conductivity, as well as ferromagnetic behavior. Namely, systematic studies of properties of nano-sized CeO_2 and other semiconductor nanostructures oxide demonstrated that oxygen vacancies play significant role in establishing both ionic conductivity and ferromagnetic behavior in these materials. When an oxygen vacancy is created in a ceria lattice, two electrons are left behind. Due to one of the widely used mechanisms ("F center exchange mechanism") for the explanation of ferromagnetic ordering in nanocrystalline CeO_2 an electron is trapped in an oxygen vacancy and acts as a coupling agent between magnetic Ce^{3+} ions [16]. Recently research [17] has shown that using SPRT method for pure nanopowder CeO_2 synthesis is promising method for exhibiting magnetism due to a significant amount of electron trapped in oxygen vacancies. Thus, it can be summarized that different synthesis methods strongly influence the formation of different kinds of oxygen-deficient defect centers with or without trapped electrons [17], which present a crucial factor for the assessment of potential electrical and ferromagnetic behavior.

Nitrogen adsorption isotherms, presented as the amount of N_2 adsorbed in the function of relative pressure at −196°C, are shown in Figure 2(a). According to the IUPAC classification [38], the isotherms of both MGNP and SPRT nanopowders are of the IV-type, with a hysteresis loop. The pore size distribution (PSD) is shown in Figure 2(a) (insets). It shows that the nanopowders obtained by the MGNP method are mesoporous. The SPRT nanopowders are also mesoporous, but with certain participation of micropores. The distribution is continuous and, for all the samples, the majority of the pore radii are below 2 nm (Figure 2(a)—inset).

The specific surface areas calculated by the BET equation (slow temperature nitrogen physisorption) are presented in Table 2. Overall specific surface areas of nanopowders obtained by the MGNP and SPRT methods are 36 and 117 $m^2 g^{-1}$, respectively. Besides, the α_s-plots (Figure 2(b)) were used for determining the surface area of various surface regions responsible for adsorption, obtained using standard nitrogen adsorption isotherms shown in Figure 2(a). The

Table 2: The textural properties of samples obtained by the MGNP and SPRT methods.

Composition	S_{BET} (m^2/g)	S_{meso} (m^2/g)	S_{micro} (m^2/g)	V_{micro} (cm^3/g)
MGNP method				
$Ce_{0.8}Nd_{0.0025}Sm_{0.0025}Gd_{0.005}Dy_{0.095}Y_{0.095}O_{2-\delta}$	36	36	—	—
SPRT method				
$Ce_{0.8}Nd_{0.0025}Sm_{0.0025}Gd_{0.005}Dy_{0.095}Y_{0.095}O_{2-\delta}$	117	35	82	0.060

slope of the straight line in the medium α_s region gives the surface area of mesopores (S_{meso}), while micropore volume (V_{micro}) is given by the intercept. Subtraction S_{meso} from S_{BET} presents the micropore surface (S_{micro}). The calculated porosity parameters (S_{meso}, S_{micro}, and V_{micro}) are presented in Table 2. These parameters show the difference between the samples obtained by the MGNP and SPRT methods. The MGNP samples have lower specific surface areas and only mesopores, while the SPRT samples have higher specific surface areas and contain both mesopores and micropores. This leads to the conclusion that the synthesis method had great influence on forming specific surfaces, as well as porosity. In addition, the powder obtained by the SPRT method retained high specific surface area, which is in agreement with small crystallite size confirmed by the XRPD and TEM analyses. Additionally, since the XRPD analysis showed that particles have small crystallite size (several nm), both micro- and mesopores could be formed during the agglomeration (Table 2), which was confirmed by the TEM and SEM methods (Section 3.2).

3.2. Morphology (TEM and SEM Analysis) and Elemental Composition (EDS Analysis). The results obtained by the TEM analysis of the $Ce_{0.8}Nd_{0.0025}Sm_{0.0025}Gd_{0.005}Dy_{0.095}Y_{0.095}O_{2-\delta}$ nanopowders synthesized using the MGNP and SPRT method are presented in Figure 3. All recordings (Figure 4) show that crystallites tended to agglomerate and form aggregates, which is consistent with the literature data [39]. Basically, nanoparticles have a natural tendency to agglomerate for two main reasons: firstly, the agglomeration is a more stable configuration from the point of view of the surface free energy, and, secondly, the nanoparticles tend to agglomerate as a consequence of the tendency of crystallite growth. This tendency was confirmed by the presence of micro- and mesopores, as shown in Table 2. Additionally, from the obtained TEM data (Table 1) it can be seen that the particle size is in the nanometric range, and its value is very similar to that obtained by the XRPD analysis. Besides, the TEM images (Figure 3) show that the fine powders are formed of more soft and microporous aggregates responsible for high specific surface area (Table 2), which can be clearly seen in the SEM images (Figure 4).

With the point of view of potential application of the synthesized nanopowders as ferromagnetic, it is important to notice that obtained micrographs (Figures 3 and 4) contain very developed grain boundaries (GBs) and free surfaces. Generally, in the last years it has been shown that GBs in oxides are the reason of ferromagnetic behavior and allow them to act as promising materials for spintronics [19, 20]. The ferromagnetic behavior has not shown in bulk oxides (even doped with ferromagnetic ions such as Fe or Co), but only in polycrystalline samples with very small grains and high specific area of grain boundaries [19]. The specific area of grain boundary represents the ratio of GB area to grain volume, and it has been shown as one of the main factors controlling ferromagnetic activities [19, 20]. Furthermore, if the specific area of grain boundary is high enough, the ferromagnetism will appear even in pure (nondoped) oxide nanopowder [19]. In our case, the specific number of dopant ions can be segregated in grain boundaries (Figures 3 and 4) and remains invisible for XRPD and TEM analysis. This leads to the conclusion that accumulation of dopant ions in grain boundaries, interphase boundaries, and amorphous surficial, interfacial, and intergranular layers can improve the ferromagnetic properties of pure CeO_2 [20]. Because the mainly amorphous grain boundary region has a range of approximately 1-2 nm in thickness [19] (magnitude of ionic radius is about 0.1 nm), it is extremely important to understand phenomena in it. Newly results suggest that the formation of unpaired electrons is possible at grain boundaries and that geometries may exist, where such electrons are coupled ferromagnetically [19]. The presented micrographs (Figures 3 and 4) show that SPRT obtained nanopowder has slightly better GBs development relative to the sample synthesized by MGNP methods. Thus, based on the previous results [17] and due to small grain size (Table 1), we believed that nanopowders $Ce_{0.8}Nd_{0.0025}Sm_{0.0025}Gd_{0.005}Dy_{0.095}Y_{0.095}O_{2-\delta}$ and the obtained MGNP and SPRT methods can be good candidates with potential ferromagnetic behavior.

The EDX microanalysis was determined from four runs for each $Ce_{0.8}Nd_{0.0025}Sm_{0.0025}Gd_{0.005}Dy_{0.095}Y_{0.095}O_{2-\delta}$ nanopowder obtained using the MGNP and SPRT methods. The corresponding EDS images (Figure 5) confirmed the incorporation of the dopant ions in the structure for all synthesized nanopowders. The mean value of the chemical ratio Ce/Nd/Sm/Gd/Dy/Y confirmed that the dopant ions in the corresponding concentrations for the MGNP sample (Ce/Nd/Sm/Gd/Dy/Y = 78.70/0.36/0.27/4.72/6.26/9.69) and SPRT sample (Ce/Nd/Sm/Gd/Dy/Y = 78.85/0.29/0.38/5.31/6.64/8.53) were successfully incorporated into the host matrix. Thus, the EDS analysis revealed that all powders had chemical composition very similar to the nominal chemical composition.

4. Conclusions

The prepared and characterized multidoped ceria $Ce_{0.8}Nd_{0.0025}Sm_{0.0025}Gd_{0.005}Dy_{0.095}Y_{0.095}O_{2-\delta}$ ($x = 0.2$) samples are new materials that were not reported until now.

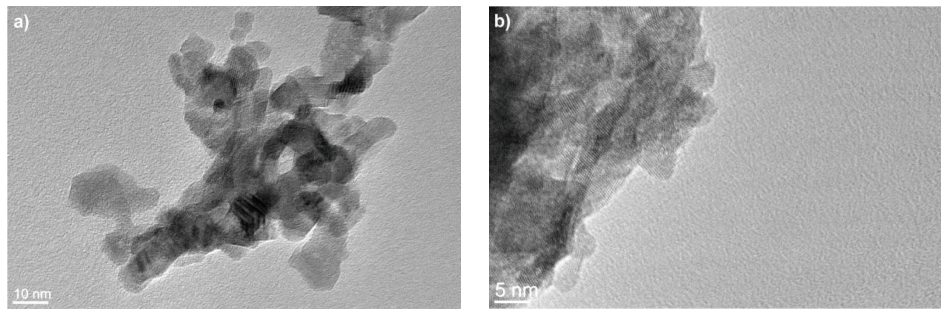

(a) (b)

Figure 3: TEM images of the $Ce_{0.8}Nd_{0.0025}Sm_{0.0025}Gd_{0.005}Dy_{0.095}Y_{0.095}O_{2-\delta}$ nanopowders obtained by the MGNP (a) and SPRT (b) methods.

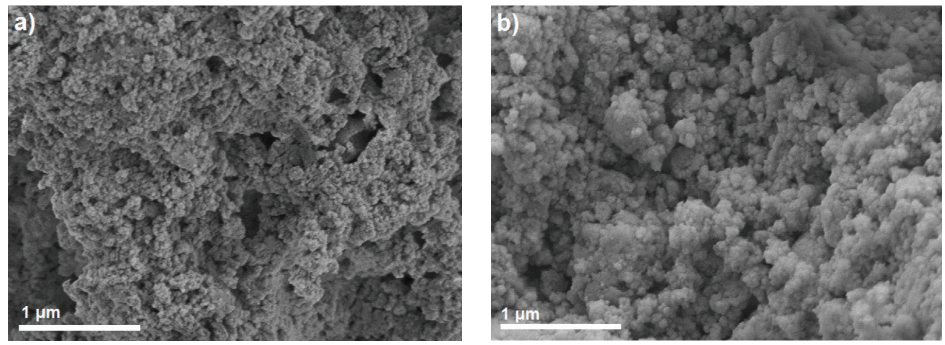

(a) (b)

Figure 4: SEM images of the $Ce_{0.8}Nd_{0.0025}Sm_{0.0025}Gd_{0.005}Dy_{0.095}Y_{0.095}O_{2-\delta}$ nanopowders obtained by the MGNP (a) and SPRT (b) methods.

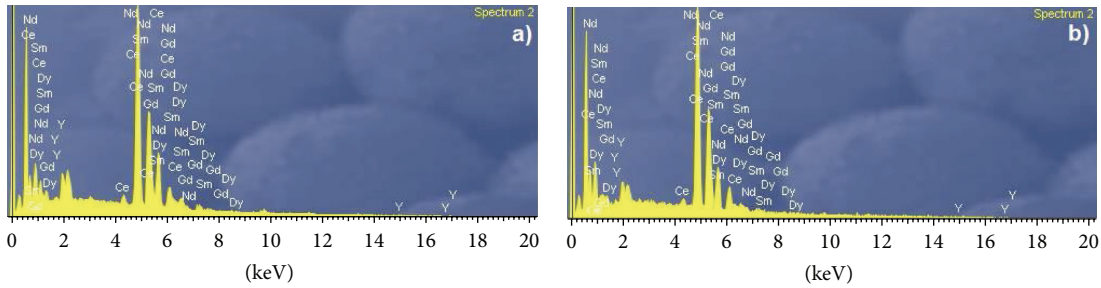

Full scale 4848 cts cursor: 0.000 Full scale 1773 cts cursor: 0.000

(a) (b)

Figure 5: EDX spectra of the $Ce_{0.8}Nd_{0.0025}Sm_{0.0025}Gd_{0.005}Dy_{0.095}Y_{0.095}O_{2-\delta}$ nanopowders obtained by the MGNP (a) and SPRT (b) methods.

The comparative characterization of synthesized multidoped nanopowders based on CeO_2 by using two different methods was successfully performed with the intention to determine differences in the powders caused by the use of different synthesis methods. Both powders were successfully synthesized by modified glycine-nitrate procedure (MGNP method) and room temperature self-propagating reaction (SPRT method) had the fluorite structure, similar to pure ceria with the space group *Fm3m*. The XRPD and TEM analyses confirmed particle size in the nanometer range. The presence of oxygen vacancies in ceria lattice, registered by Raman spectroscopy, indicated potential improvement of the ionic conductivity and ferromagnetic behavior. The TEM and SEM analysis show the very developed grain boundaries and free surfaces of presented powders and allow them to act as ferromagnetic. Thus, taking into account the properties of the obtained nanopowders and very easy and inexpensive synthesis procedures, their potential as suitable electrolytes for solid oxide fuel cells, as well as for potential applications in spintronics, might be regarded as high.

Competing Interests

The authors declare that they have no competing interests.

Acknowledgments

This work was supported by the Ministry of Education, Science and Technological Development of the Republic of Serbia (Project nos. III 45012, III 45007, and 172015). The authors are also grateful to A. von Humboldt Foundation for supporting this work.

References

[1] W. Liu, B. Li, H. Liu, and W. Pan, "Electrical conductivity of textured $Sm3^+$ and $Nd3^+$ Co-doped CeO_2 thin-film electrolyte," *Electrochimica Acta*, vol. 56, no. 9, pp. 3334–3337, 2011.

[2] D. Pérez-Coll, P. Núñez, and J. R. Frade, "The role of SiO_2 and sintering temperature on the grain boundary properties of $Ce_{0.8}Sm_{0.2}O_{2-\delta}$," *Journal of Power Sources*, vol. 196, no. 20, pp. 8383–8390, 2011.

[3] L. Truffault, M.-T. Ta, T. Devers et al., "Application of nanostructured Ca doped CeO_2 for ultraviolet filtration," *Materials Research Bulletin*, vol. 45, no. 5, pp. 527–535, 2010.

[4] M. Aguirre, M. Paulis, and J. R. Leiza, "UV screening clear coats based on encapsulated CeO_2 hybrid latexes," *Journal of Materials Chemistry A*, vol. 1, no. 9, pp. 3155–3162, 2013.

[5] T. Suratwala, R. Steele, M. D. Feit et al., "Effect of rogue particles on the sub-surface damage of fused silica during grinding/polishing," *Journal of Non-Crystalline Solids*, vol. 354, no. 18, pp. 2023–2037, 2008.

[6] C. Li, X. Zhang, W. Dong, and Y. Liu, "High photocatalytic activity material based on high–porosity ZnO/CeO_2 nanofibers," *Materials Letters*, vol. 80, pp. 145–147, 2012.

[7] P. Panagiotopoulou, J. Papavasiliou, G. Avgouropoulos, T. Ioannides, and D. I. Kondarides, "Water-gas shift activity of doped Pt/CeO_2 catalysts," *Chemical Engineering Journal*, vol. 134, no. 1–3, pp. 16–22, 2007.

[8] H. Li, G. Lu, Y. Wang, Y. Guo, and Y. Guo, "Synthesis of flower-like la or Pr-doped mesoporous ceria microspheres and their catalytic activities for methane combustion," *Catalysis Communications*, vol. 11, no. 11, pp. 946–950, 2010.

[9] H.-T. Chen, "First-principles study of CO adsorption and oxidation on Ru-doped CeO_2(111) surface," *Journal of Physical Chemistry C*, vol. 116, no. 10, pp. 6239–6246, 2012.

[10] X. Ma, X. Feng, X. He et al., "Mesoporous CuO/CeO_2 bimetal oxides: one-pot synthesis, characterization and their application in catalytic destruction of 1,2-dichlorobenzene," *Microporous and Mesoporous Materials*, vol. 158, pp. 214–218, 2012.

[11] D. H. Leea, K. S. Chaa, Y. S. Leea, K. S. Kangb, C. S. Parkb, and Y. H. Kima, "Effects of CeO_2 additive on redox characteristics of Febased mixed oxide mediums for storage and production of hydrogen," *International Journal of Hydrogen Energy*, vol. 34, no. 3, pp. 1417–1422, 2009.

[12] R. Chockalingam, A. K. Ganguli, and S. Basu, "Praseodymium and gadolinium doped ceria as a cathode material for low temperature solid oxide fuel cells," *Journal of Power Sources*, vol. 250, pp. 80–89, 2014.

[13] J. Jiang, W. Shen, and J. L. Hertz, "Structure and ionic conductivity of nanoscale gadolinia-doped ceria thin films," *Solid State Ionics*, vol. 249-250, pp. 139–143, 2013.

[14] Z. D. Dohčević-Mitrović, N. Paunović, M. Radović et al., "Valence state dependent room–temperature ferromagnetism in Fe–doped ceria nanocrystals," *Applied Physics Letters*, vol. 96, no. 20, pp. 203104–203107, 2010.

[15] S. Phokha, S. Pinitsoontorn, P. Chirawatkul, Y. Poo-Arporn, and S. Maensiri, "Synthesis, characterization, and magnetic properties of monodisperse CeO_2 nanospheres prepared by PVP-assisted hydrothermal method," *Nanoscale Research Letters*, vol. 7, pp. 425–438, 2012.

[16] N. Paunović, Z. Dohcevic-Mitrovic, R. Scurtu et al., "Suppression of inherent ferromagnetism in Pr-doped CeO_2 nanocrystals," *Nanoscale*, vol. 4, no. 17, pp. 5469–5476, 2012.

[17] S. Aškrabić, Z. D. Dohčević-Mitrović, V. D. Araújo, G. Ionita, M. M. De Lima, and A. Cantarero, "F-centre luminescence in nanocrystalline CeO_2," *Journal of Physics D: Applied Physics*, vol. 46, no. 49, pp. 495306–495315, 2013.

[18] S. Tsunekawa, T. Fukuda, and A. Kasuya, "X-ray photoelectron spectroscopy of monodisperse CeO_{2-x} nanoparticles," *Surface Science*, vol. 457, no. 3, pp. L437–L440, 2000.

[19] T. Tietze, P. Audehm, Y.-C. Chen et al., "Interfacial dominated ferromagnetism in nanograined ZnO: a μSR and DFT study," *Scientific Reports*, vol. 5, pp. 8871–8877, 2015.

[20] B. B. Straumal, A. A. Mazilkin, S. G. Protasova et al., "Grain boundaries as a source of ferromagnetism and increased solubility of Ni in nanograined ZnO," *Reviews on Advanced Materials Science*, vol. 41, no. 1, pp. 61–71, 2015.

[21] A. R. West, *Solid State Chemistry and Its Applications*, John Wiley & Sons, New York, NY, USA, 1991.

[22] S. E. Dann, *Reactions and Characterization of Solids*, Wiley, New York, NY, USA, 2000.

[23] S. Wang, K. Maeda, and M. Awano, "Direct formation of crystalline gadolinium–doped ceria powder via polymerized precursor solution," *Journal of the American Ceramic Society*, vol. 85, no. 7, pp. 1750–1752, 2002.

[24] M. Stojmenović, S. Bošković, S. Zec et al., "Characterization of nanometric multidoped ceria powders," *Journal of Alloys and Compounds*, vol. 507, no. 1, pp. 279–285, 2010.

[25] M. Stojmenovic, S. Bokovic, M. M. Unic et al., "Studies on structural, morphological and electrical properties of $Ce_{1-x}Er_xO_{2-\delta}$ (x = 0.05–0.20) as solid electrolyte for IT-SOFC," *Materials Chemistry and Physics*, vol. 153, pp. 422–431, 2015.

[26] M. Stojmenović, M. Žunić, J. Gulicovski et al., "Structural, morphological, and electrical properties of doped ceria as a solid electrolyte for intermediate–temperature solid oxide fuel cells," *Journal of Materials Science*, vol. 50, no. 10, pp. 3781–3794, 2015.

[27] M. Stojmenović, M. C. Milenković, P. T. Banković et al., "Influence of temperature and dopant concentration on structural, morphological and optical properties of nanometric $Ce_{1-x}Er_xO_{2-\delta}$ ($x = 0.05$–0.20) as a pigment," *Dyes and Pigments*, vol. 123, pp. 116–124, 2015.

[28] C. Suryanarayana and M. Grant Norton, *X-Ray Diffraction: A Practical Approach*, Springer, New York, NY, USA, 1998.

[29] E. P. Barrett, L. G. Joyner, and P. P. Halenda, "The determination of pore volume and area distributions in porous substances. I. Computations from nitrogen isotherms," *Journal of the American Chemical Society*, vol. 73, no. 1, pp. 373–380, 1951.

[30] K. Kaneko, C. Ishii, M. Ruike, and H. kuwabara, "Origin of superhigh surface area and microcrystalline graphitic structures of activated carbons," *Carbon*, vol. 30, no. 7, pp. 1075–1088, 1992.

[31] M. Kruk, M. Jaroniec, and K. P. Gadkaree, "Nitrogen adsorption studies of novel synthetic active carbons," *Journal of Colloid and Interface Science*, vol. 192, no. 1, pp. 250–256, 1997.

[32] K. Kaneko, C. Ishii, H. Kanoh, Y. Hanzawa, N. Setoyama, and T. Suzuki, "Characterization of porous carbons with high resolution α_s-analysis and low temperature magnetic susceptibility," *Advances in Colloid and Interface Science*, vol. 76-77, pp. 295–320, 1998.

[33] R. D. Shannon, "Revised effective ionic radii and systematic studies of interatomic distances in halides and chalcogenides," *Acta Crystallographica Section A*, vol. 32, no. 5, pp. 751–767, 1976.

[34] S. Tsunekawa, J.-T. Wang, and Y. Kawazoe, "Lattice constants and electron gap energies of nano- and subnano-sized cerium oxides from the experiments and first-principles calculations," *Journal of Alloys and Compounds*, vol. 408–412, pp. 1145–1148, 2006.

[35] S. Tsunekawa, K. Ishikawa, Z.-Q. Li, Y. Kawazoe, and A. Kasuya, "Origin of anomalous lattice expansion in oxide nanoparticles," *Physical Review Letters*, vol. 85, no. 16, pp. 3440–3443, 2000.

[36] F. Zhang, S.-W. Chan, J. E. Spanier et al., "Cerium oxide nanoparticles: size-selective formation and structure analysis," *Applied Physics Letters*, vol. 80, no. 1, pp. 127–129, 2002.

[37] J. R. Bridge, K. S. Hass, B. D. Poindexter, and W. H. Weber, "Raman and X–ray studies of $Ce_{1-x}RE_xO_{2-y}$, where REL'La, Pr, Nd, Eu, Gd and Tb," *Journal of Applied Physics*, vol. 76, pp. 2435–2441, 1994.

[38] K. S. W. Sing, D. H. Everett, R. A. W. Haul et al., "Reporting physisorption data for gas/solid systems with special reference to the determination of surface area and porosity," *Pure and Applied Chemistry*, vol. 54, no. 11, pp. 2201–2218, 1982.

[39] S. Phoka, P. Laokul, E. Swatsitang, V. Promarak, S. Seraphin, and S. Maensiri, "Synthesis, structural and optical properties of CeO_2 nanoparticles synthesized by a simple polyvinyl pyrrolidone (PVP) solution route," *Materials Chemistry and Physics*, vol. 115, no. 1, pp. 423–428, 2009.